INTELLIGENT CABLE FAULT DETECTION TECHNOLOGY CONSIDERING CURRENT HARMONIC CHARACTERISTICS

Yuning-Tao*

- College of Electrical Engineering and New Energy, China Three Gorges University, Yichang, Hubei, 443000, China
- taoyuning12@163.com

Reception: 8 April 2024 | **Acceptance**: 6 May 2024 | **Publication**: 8 June 2024

Suggested citation:

Yuning-Tao. (2024). **Intelligent cable fault detection technology considering current harmonic characteristics.** *3C Tecnología. Glosas de Innovación aplicadas a la pyme. 13(1)*, 99-128. https://doi.org/10.17993/3ctecno.2024.v13n1e45.99-128

https://doi.org/10.17993/3ctecno.2024.v13n1e45.99-128

ABSTRACT

With the rapid development of the power system, cable faults have become an important factor affecting the stable operation of the power system. In this paper, for the problem of cable faults, we improve the overshoot, undershoot phenomenon and sieve speed of the envelope fitting in the Hilbert-Huang transform algorithm, and extract the harmonic characteristics of the current of cable faults by using the improved HHT model. Then, we utilize the information entropy and wavelet singular entropy algorithm to integrate semi-parametric support vector machine algorithm, S-SVM, and construct the wavelet singular entropy and S-SVM model. The information entropy and wavelet singular entropy algorithms are fused with semiparametric support vector machine algorithm, S-SVM, and constructed into wavelet singular entropy and S-SVM models, which are applied to the cable fault identification experiments for detecting different faults in cables. The experimental results show that, when the cables are short-circuited, the currents of different short-circuited cables are all lower than the normal currents, and the wavelet singular entropy and S-SVM models reach more than 92% of the accuracy of the identification of the degradation of the cable line and short-circuited faults. The accuracy of the wavelet singular entropy and S-SVM model for the identification of cable line deterioration and short circuit faults reaches more than 92%, and the overall cable fault detection reaches 98.04%.The maximum error value of the wavelet singular entropy and S-SVM model for detection is 0.5329, and there are only two groups of data more than 0.5.The algorithms in this paper are able to detect the various localization of the cable faults quickly and accurately, and they have a high practical value.

KEYWORDS

HHT algorithm; Wavelet singular entropy; S-SVM model; Current harmonic characteristics; Fault detection

https://doi.org/10.17993/3ctecno.2024.v13n1e45.99-128

INDEX

ABSTRACT **2**

KEYWORDS **2**

1. INTRODUCTION **4**

2. CONSTRUCTION OF INTELLIGENT CABLE FAULT DETECTION MODEL **7**

2.1. Construction of Improved Hilbert-Huang Transform Models 7

2.1.1. Hilbert-Huang transform algorithm 7

2.1.2. Improvement of Envelope Fitting Algorithm 10

2.1.3. Improved HHT algorithm flow 12

2.2. Construction of wavelet-based singular entropy sum and S-SVM network models 14

2.2.1. Semiparametric Support Vector Machines 14

2.2.2. Semi-parametric support vector machines based on least squares 15

2.2.3. Sparse greedy matrix approximation 15

2.2.4. Iterative reweighted least squares 17

2.2.5. Wavelet Transform 18

2.2.6. Shannon information entropy and wavelet singular entropy 19

2.2.7. Cable fault detection strategy based on wavelet singular entropy and S-SVM models 20

3. ANALYSIS OF INTELLIGENT CABLE FAULT DETECTION RESULTS CONSIDERING CURRENT HARMONIC FEATURES **21**

3.1. Analysis of intelligent detection results of cable line deterioration faults 21

3.1.1. Harmonic feature extraction for cable line degradation 21

3.1.2. Analysis of cable line deterioration identification test results 22

3.2. Analysis of intelligent detection results of cable short-circuit faults 24

3.2.1. Cable short circuit fault analysis 24

3.2.2. Harmonic feature extraction for cable short-circuit faults 26

3.2.3. Identification and detection results of cable short-circuit faults 27

3.3. Analysis of intelligent detection results of cable faults 28

4. CONCLUSION **28**

REFERENCES **29**

https://doi.org/10.17993/3ctecno.2024.v13n1e45.99-128

1. INTRODUCTION

Power resources have become one of the most important energy sources in China, the rapid increase in the consumption of electric power resources in small, medium and large cities, in order to meet the needs of the masses of electricity, widely used power cables as a transmission tool and connecting lines [1-2]. the current development of China's electric power industry projects continue to increase, in order not to take up too much land resources, cables are usually generally buried in the ground, which increases the difficulty of troubleshooting power cable faults to a certain extent. If the maintenance work is not timely, then it is easy to increase the probability of power outages, bringing difficulties to the people's lives, directly affecting people's production and life [3-4]. combined with the current social development trend in China, the most critical type of power system failure is cable failure, to ensure the stability and safe operation of China's power system, it is necessary to carry out power cable failure at the first time, the power cable failure is the most critical type of power cable failure. To ensure the stable and safe operation of China's power system, it is necessary to carry out power cable fault inspection and testing at the first time, accurately put forward the cable inspection method, and effectively put forward the measures to solve the fault, repair the power cable faults, so as to promote the stability and safety of the power project [5-6].

In order to reduce the use of land resources, to bring higher economic benefits, so the cable is usually buried in the ground, but this to a certain extent also brings certain problems, due to the cable buried deep underground, if a fault occurs, it is difficult to investigate, which increases the difficulty of investigation [7-8]. In the detection of cable faults, the principle that must be adhered to is to be green, while maximizing the economic benefits, not only to require the practicality of strong, but also to ensure that the scientific nature of the use of advanced technology to fully reduce losses, and constantly improve the efficiency of the power grid in the operation of the power industry to a certain extent will promote the progress and development of China's electric power industry, and play a huge significance of the promotion of the [9-10].

With the continuous development of the market economy, people's living standards continue to improve, the structure of the urban power grid is more complex, the number of cables in use is increasing day by day. the safety of the cable operation, directly on the power system to bring a direct impact on the cable management and maintenance of the power sector has become the focus of the attention of the electric power sector. Baranowski, J. and other researchers proposed a new method to detect different signals based on the depth distribution of the Bayesian function to diagnose cable faults, the results of the study confirm that the method has great potential for diagnosis in unknown situations [11]. Liu, X. and other researchers designed a short cable line fault location method based on the theory of transmission line and the circuit theorem, and the test was carried out on 50 coaxial cables, and the test verified that the accuracy of this method is not affected by the impedance of faults and the terminating impedance [12]. Xuebin, Q. and other researchers proposed an on-line cable fault diagnosis method to address the need for on-line diagnosis of cable faults,

https://doi.org/10.17993/3ctecno.2024.v13n1e45.99-128

which is more advantageous than the traditional shallow neural network-based cable fault identification method [13]. Cataldo, A. C. G. described the time-domain reflectance (TDR) based localization method along the permittivity variations (DPVs) of cable systems, and pointed out that due to the increase in the number of DPVs, the fault location is not as accurate as the fault impedance and termination impedance of the cable system. It was pointed out that increasing the pulse width to study the localization of cables over longer distances leads to focusing on different TDR reflectance maps each time, which is very time-consuming and does not guarantee optimal performance [14].Wang, F. and other researchers envisioned a fault diagnostic method based on the BP-Adaboost algorithm to solve the problem of faults on aeronautical cables, and the results of the algorithm were studied by using the Matlab software for analysis and example feedback to validate the results. Matlab software is used to analyze the algorithm results and feedback examples to verify the feasibility of the proposed fault diagnosis method [15]. Sian, H. W. and other researchers designed a hybrid diagnostic algorithm based on the Discrete Wavelet Transform (DWT) and Symmetric Dot Plot (SDP) analysis of Convolutional Probabilistic Neural Networks (CPNN) to solve the insulation faults in XLPE cables. Simulation tests show that the accuracy of this method is more than 96%, and the accuracy of this method is higher than 96%. Simulation tests have shown that the method can diagnose power cable faults with an accuracy of more than 96% and a short detection time, which makes it fully capable of detecting insulation faults in cables [16]. Marriott, N. discusses the role and advantages of Megger's new SMART THUMP ST25-30 Portable Cable Tester, which provides an automated test sequence with the ability to identify, prelocate, and pinpoint cable faults, and to automatically supplement the interpretation of the test results. Non-specialized users can obtain reliable results in a safe and easy way [17]. Lowczowski, K. and other researchers analyzed the application of cable shielding currents in the identification and location of ground faults, and in this way gave phase ground fault currents in different power system configurations, in order to test the ability to detect faults based on the above principles, and proved the reliability of this method for fault detection. Finally, a solution to improve the localization capability is proposed, and the feasibility of the improved solution is confirmed by simulation tests with PSCAD software [18]. Hu, C. and other researchers investigate the ship cable fault information acquisition model based on the automatic identification technology, and simulation tests are conducted to confirm the feasibility of the Hilbert-Huang Transform (HHT) to automatically identify cable faults, and to construct an automatic cable fault information acquisition model [19]. Lai, Q. and other researchers studied the 110kv transmission line cable terminal tail pipe breakdown fault, and give the cable installation improvement measures to reduce the probability of cable terminal breakdown faults, and after simulation and disassembly test, the feasibility analysis, for similar cable faults, is carried out. The feasibility analysis is carried out to provide important reference opinions for the investigation and solution of similar cable faults [20]. Liu, N. and other researchers conceived a deep neural network-based cable fault signal classification and identification method to accurately identify the early cable fault problems, and the reliability of the method is demonstrated through experiments [21]. Wang, Y. and other

https://doi.org/10.17993/3ctecno.2024.v13n1e45.99-128

researchers designed a method based on the constrained Boltzmann machine (Wang, Y. and other researchers designed a cable early fault identification method based on Restricted Boltzmann Machine (RBM) and Stacked Auto-Encoder (SAE), which demonstrated higher accuracy after simulation tests comparing with traditional methods such as convolutional neural networks [22]. A new algorithm for accurate location of early faults in underground cables using double-ended synchronized zero sequence waveforms was proposed by Qu, K. et al. A large number of simulation experiments were conducted at PSCAD/EMTDC to support the accuracy and reliability of the algorithm [23]. Kwon, G. Y. et al. discussed an improved fault localization technique, instantaneous frequency-domain reflectance and tangent-distance pattern recognition, for fault diagnosis and protection of cables, and simulation data verified that this method can improve the reliability of high-voltage DC power systems. For fault diagnosis and protection of cables, and simulated test data verified that this method can improve the reliability of HVDC power systems [24].

In this paper, the Hilbert transform is applied to the IMF components to obtain the Hilbert-Huang transform model, and then the local extreme points are densified by using the cut-contact mean points, and then the interpolated curve segments are spliced by the segmented power function to improve the insufficiency of the envelope fitting in the HHT transform model, and then the current harmonic characteristics of the cable faults are extracted and analyzed, and the wavelet singularity is obtained by combining the wavelet transform with the information entropy. The wavelet singular entropy is obtained by combining the information entropy and wavelet transform, which is integrated into the S-SVM algorithm, and the sparse greedy matrix approximation is used to select the basic element set, and the iterative reweighted least squares algorithm is introduced to iterate and optimize the S-SVM model, which finally constitutes the wavelet singular entropy and the S-SVM model. the signal is decomposed by the wavelet singular entropy and the signal components are extracted, and the extracted current harmonic features are screened and reconstructed, and the current harmonic features are extracted and analyzed. After that, the extracted current harmonic feature vectors are filtered and reconstructed, and then the cable fault samples are input to the S-SVM model for training, and finally the wavelet singular entropy and S-SVM models are realized to accurately identify different faults of cables.

https://doi.org/10.17993/3ctecno.2024.v13n1e45.99-128

2. CONSTRUCTION OF INTELLIGENT CABLE FAULT DETECTION MODEL

2.1. CONSTRUCTION OF IMPROVED HILBERT-HUANG TRANSFORM MODELS

2.1.1. HILBERT-HUANG TRANSFORM ALGORITHM

The HHT algorithm is to sieve the various frequency components or trends contained in the signal layer by layer in order to obtain a series of IMF components containing different feature information, and then these IMF components are subjected to the Hilbert transform, which can obtain the Hilbert spectra and the marginal spectra, and then obtain the amplitude distribution pattern of the signal in the spatial or temporal scale.

1. Instantaneous frequency

In the process of analyzing nonlinear signals, the instantaneous characteristics have a very important role, in the traditional Fourier transform, less than a wavelength signal will not be able to give the definition of the frequency, that is, it cannot be used to accurately describe the instantaneous parameters of the non-smooth signal, the instantaneous frequency mentioned in the Hilbert transform has the actual physical meaning, and the basic definition of the frequency is consistent.

When analyzing a smooth signal, the frequency of the signal refers to the f in the Fourier transform.

$$X(f) = \int_{-\infty}^{\infty} x(t)e^{-j\pi ft}dt \tag{1}$$

In the formula f, becomes the Fourier frequency, and the time is not related.

When analyzing non-stationary signals, the instantaneous frequency changes with time, and it is not possible to accurately describe the changing frequency, the Fourier frequency loses its significance, so a new definition of the instantaneous frequency is needed to describe this change.

Let $X(t)$ be a signal of any time series, $Y(t)$ is the Hilbert transform of the signal, then $Y(t)$ can be expressed by $X(t)$ as follows.

$$Y(t) = \frac{1}{\pi}\int_{-\infty}^{\infty} \frac{X(t)}{t-\tau}d\tau \tag{2}$$

Meanwhile, $X(t)$ can be expressed by $Y(t)$ as follows:

https://doi.org/10.17993/3ctecno.2024.v13n1e45.99-128

$$X(t) = \frac{1}{\pi}\int_{-\infty}^{\infty}\frac{Y(t)}{\tau - t}d\tau \tag{3}$$

From the above two equations, we can know that $X(t)$ and $Y(t)$ are complex conjugate pairs, and $X(t)$ and $Y(t)$ are correlated with the time series, so we can get the following analyzed signals.

$$Z(t) = X(t) + jY(t) = A(t)e^{j\theta(t)} \tag{4}$$

$$A(t) = \sqrt{X^2(t) + Y^2(t)} \tag{5}$$

$$\theta(t) = \arctan\left(\frac{Y(t)}{X(t)}\right) \tag{6}$$

Where $A(t)$ is the instantaneous amplitude and $\theta(t)$ is the phase. another instantaneous parameter is known from the phase and frequency.

$$f(t) = \frac{1}{2\pi}\frac{d\theta(t)}{dt} \tag{7}$$

As can be seen from the above equation, the Hilbert transform obtains a unique function, $Y(t)$ is the convolution of the Hilbert transform with $X(t)$ and $\frac{1}{t}$, which emphasizes the limitation of the characteristics of $X(t)$ The three instantaneous parameters of the signal can be found out through the Hilbert transform, i.e., the instantaneous amplitude, the instantaneous phase, and the instantaneous frequency. Each of the parameters is analytic, thus, the Hilbert transform has a real-life instantaneous characteristic.

2. Intrinsic Modal Functions

In general, a data often contains more than one oscillation mode, a simple Hilbert transform can not be decomposed into all the frequencies of a signal, so the data must first be decomposed into the intrinsic modal function. the definition of the instantaneous frequency of a signal needs to have the following necessary conditions, firstly, in the entire data segment, the function is symmetric, and secondly, the number of zeros and the number of extrema are the same, and finally, the local mean value of the signal is zero. Finally, the signal is locally zero-mean.

N.E. Huang defined that the intrinsic modal function must satisfy the following two conditions.

One is that the number of zero crossing points and the number of extreme points in the signal data are the same or differ by at most one.

https://doi.org/10.17993/3ctecno.2024.v13n1e45.99-128

One is that the average value of the upper and lower envelopes formed by the local extreme value points and the local extreme value points of the IMF at any moment is zero, i.e., the local signal is symmetric about the time axis.

3. Empirical modal decomposition method

Empirical modal decomposition (EMD) method is the essence of the Hilbert-Huang transform, this method is a non-stationary complex signal from the separation of several IMF process, the process is known as the screening process, screened out of the various components superimposed on the actual data series. at any time, most of the signals are unable to meet the conditions of the IMF, so it is necessary to screen the signal first and then use the Hilbert transform on the signal. At any moment, most of the signals cannot meet the conditions of IMF, so the signals need to be filtered first and then processed by Hilbert transform for each IMF component, each IMF can be linear or nonlinear.

The decomposition process is based on three assumptions: one is that the time-domain characteristics are determined by the interval between the maxima and minima, two is that the original signal should have at least one maxima and one minima, three is that if the original signal contains only inflection points, the maxima and minima can be calculated by taking the first derivative or multiple derivatives of the signal, and then the signal can be reduced by integrating the signal. The specific steps of the empirical mode decomposition are as follows.

The first step is to write the original signal as $X(t)$, determine all the maximum and minimum value points of $X(t)$, and fit the maximum value points to the upper envelope with the three times spline sampling function, and the minimum value points to the lower envelope with the three times spline sampling function, and the upper and lower envelopes should contain all the data.

In the second step, the average value of the upper and lower envelopes is calculated and denoted as m_1, and the original signal X(t), is subtracted from m_1 to obtain a new sequence h_1.

$$h_1 = X(t) - m_1 \tag{8}$$

In this decomposition, the low-frequency quantities of the signal are separated out, and h_1 is the high-frequency quantity of the signal. Ideally, if h_1 satisfies the two necessary conditions of IMF, then h_1 is the first IMF component of the original signal $X(t)$, and is denoted as $c_1 = h_1$.

In the third step, if the high-frequency quantity h_1 does not satisfy the two necessary conditions of IMF, then h_1 is continued as the original signal, repeat the above two steps, first calculate the average value of h_1, denoted as m_{11}, and then calculate $h_{11} = h_1 - m_{11}$, and judge whether h_{11} satisfies the two necessary conditions of IMF, if it does, then h_{11} is denoted as c_1, if it doesn't, then continue to

https://doi.org/10.17993/3ctecno.2024.v13n1e45.99-128

calculate, and repeat the cycle of the first and the second steps, until the obtained h_{1k} satisfies the two necessary conditions and is denoted as $c_1 = h_{1k}$, and c_1 is the first IMF component of the original signal $X(t)$.

In the fourth step, c1, is separated from the original signal $X(t)$ to obtain a signal that removes the high-frequency quantityv c_1, denoted as r_1.

$$r_1 = X(t) - c_1 \tag{9}$$

The r_1 signal as the original signal, repeat the above steps, until we get a component that meets the two necessary conditions of IMF, which is recorded as c_2, and have been so looped n times, we can get the n IMF components of the original signal $X(t)$, as shown in Eq. (10).

$$\begin{cases} r_1 - c_2 = r_2 \\ \vdots \\ r_{n-1} - c_n = r_n \end{cases} \tag{10}$$

In the fifth step, the loop to the end, there is a residual r_n, the end of the loop termination conditions for the residual r_n is a monotonic function, that is, can no longer be extracted from it to meet the two necessary conditions of the IMF components, the end of the decomposition. the final decomposition of the form as shown in Equation (11).

$$X(t) = \sum_{i=1}^{n} c_i(t) + r_n \tag{11}$$

Where c_1 is the IMF of the original signal and r_n is a residual that converges to a constant.

2.1.2. IMPROVEMENT OF ENVELOPE FITTING ALGORITHM

When the upper and lower envelopes of the signal are approximately symmetric, it is inappropriate to use the upper and lower envelopes to find the average envelope, and for the problems of overshoot, undershoot and sieving speed in the process of EMD, this paper proposes to firstly use the tangent mean point to densify the local extreme point, and then use the segment power function to interpolate and fit the tangent mean point and local extreme point, and finally splice the interpolated curve segments together, which is the final average envelope. Then the segmented power function is used to fit the interpolation of the tangential mean and local extreme points, and finally the interpolated curve segments are spliced together, which is the final mean envelope.

1. Tangential mean points

https://doi.org/10.17993/3ctecno.2024.v13n1e45.99-128

Since the density of the distribution of the points to be interpolated directly determines the interpolation accuracy and fitting effect, the densification of the extreme points by the tangent mean points can optimize the fitting effect, and then inhibit or eliminate the overshooting and undershooting phenomena in the envelope fitting.

All the local extreme points are arranged in a time series, notated as $p\left(t_1, y_1\right), p\left(t_2, y_2\right), \ldots, p\left(t_n, y_n\right)$, where t_i is the moment when the extreme point appears, and y_i is the amplitude of the extreme point. Let $p\left(t_{i-1}, y_{i-1}\right), p\left(t_i, y_i\right), p\left(t_{i+1}, y_{i+1}\right)$ be the three neighboring extreme points, and the tangent touching the mean point is shown in Eq. (12).

$$P\left(t_i, y_i\right)=\frac{1}{2}\left[p\left(t_i, y_i\right)+\frac{t_i-t_{i-1}}{t_{i+1}-t_{i-1}} p\left(t_{i+1}, y_{i+1}\right)+\frac{t_{i+1}-t_i}{t_{i+1}-t_{i-1}} p\left(t_{i-1}, y_{i-1}\right)\right] \quad (12)$$

Where, $p\left(t_i, y_i\right)$ is the extreme point of the signal, $P\left(t_i, y_i\right)$ denotes the tangential mean point.

2. Segmental power function interpolation

Set the point to be interpolated as $P\left(t_1, y_1\right), P\left(t_2, y_2\right), \ldots, P\left(t_n, y_n\right), y=f(x)$ as the interpolation function, and use the segmented power function to interpolate any three neighboring points $P\left(t_{i-1}, y_{i-1}\right), P\left(t_i, y_i\right), P\left(t_{i+1}, y_{i+1}\right)$.

$$Q_i=\frac{\left(t_{i+1}-t_{i-1}\right)\left(y_{i-1}-y_i\right)-\left(t_{i-1}-t_i\right)\left(y_{i+1}-y_{i-1}\right)}{t_{i+1}-t_{i-1}}. \quad (13)$$

The interpolation function $f_i(t)$ satisfies equation (14).

$$\begin{cases} f_i(t)=\left(\frac{t-t_i}{t_{i-1}-t_i}\right)^\beta Q_i+\frac{y_{i+1}-y_{i-1}}{t_{i+1}-t_{i-1}}\left(t-t_i\right)+y_i, t \leq t_i, \\ f_i(t)=\left(\frac{t-t_i}{t_{i+1}-t_i}\right)^\beta Q_i+\frac{y_{i+1}-y_{i-1}}{t_{i+1}-t_{i-1}}\left(t-t_i\right)+y_i, t \geq t_i . \end{cases} \quad (14)$$

The value curve is shown in equation (15).

$$f_{i, i+1}(t)=\frac{t_{i+1}-t}{t_{i+1}-t_i} f_i(t)+\frac{t-t_i}{t_{i+1}-t_i} f_{i+1}(t) . \quad (15)$$

$f(t) IMF$

Finally, the interpolated line segments are spliced together to obtain the mean envelope, which is constructed by the segmented cubic function after many experiments and comparisons.

https://doi.org/10.17993/3ctecno.2024.v13n1e45.99-128

2.1.3. IMPROVED HHT ALGORITHM FLOW

The theory of the HHT algorithm and the operation of the specific improvement measures have been introduced, the improved HHT algorithm flowchart is shown in Fig. 1. firstly, after inputting the signal $x(t)$, find out all the local maxima and minima contained in the signal $x(t)$, and then use the cubic spline interpolation method to construct the envelope of the local maxima and minima, and then find out the average value of the envelope. If the $f(t)$ meets the condition of IMF component, then find out the energy of the remaining signal and proceed to the next step, if not, then re-screen repeatedly until the condition of IMF can be determined, and repeat the above steps until there is only one extreme point, then stop iterating.

https://doi.org/10.17993/3ctecno.2024.v13n1e45.99-128

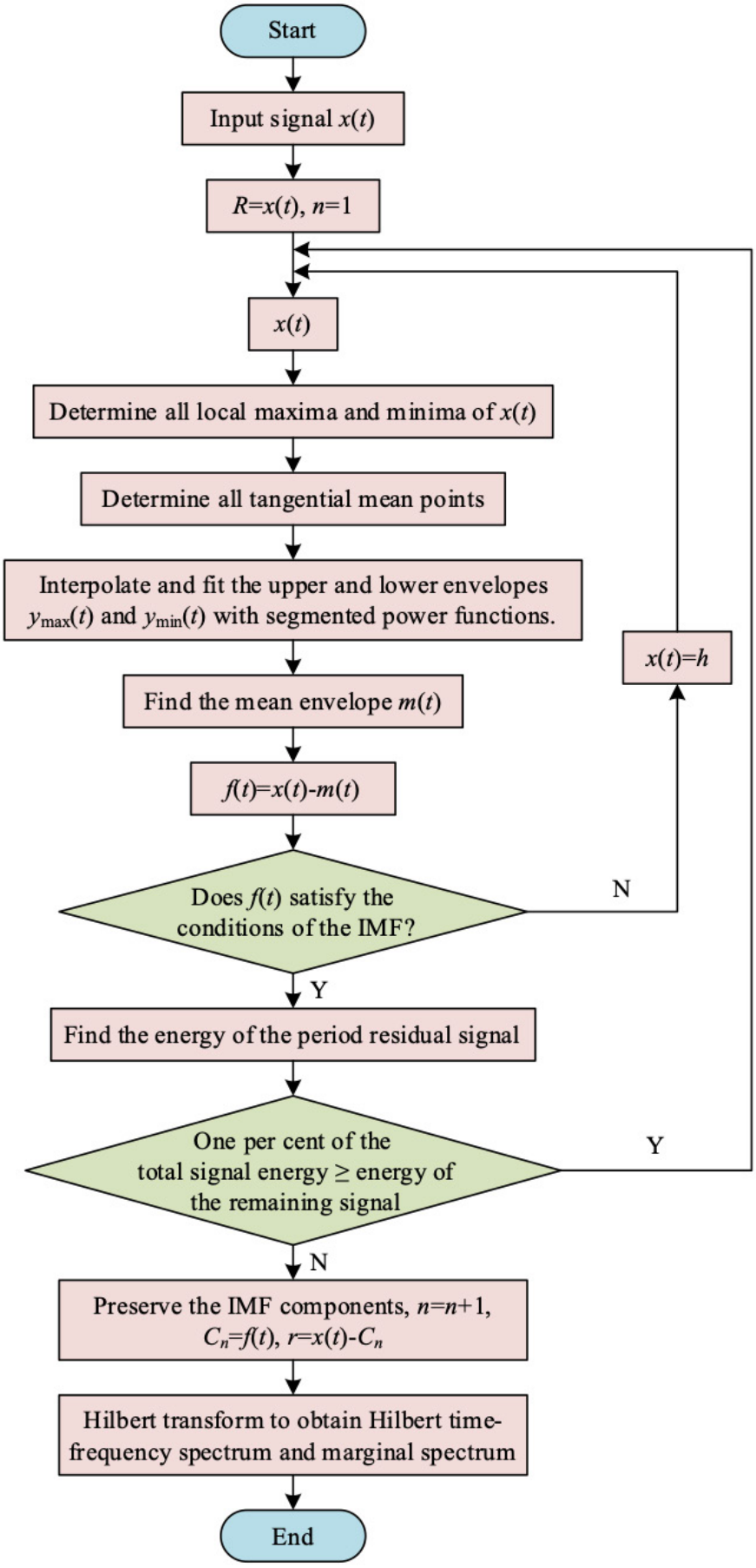

Figure 1 HHT algorithm improves the process

https://doi.org/10.17993/3ctecno.2024.v13n1e45.99-128

2.2. CONSTRUCTION OF WAVELET-BASED SINGULAR ENTROPY SUM AND S-SVM NETWORK MODELS

2.2.1. SEMIPARAMETRIC SUPPORT VECTOR MACHINES

Semi-parametric support vector machine, S-SVM, perfectly combines the advantages of parametric and non-parametric support vector machines, and improves the computational efficiency. Compared with linear support vector machine, S-SVM can handle non-linear sample data, and has better classification performance than non-linear support vector machine using soft intervals. S-SVM can avoid the problem of slow classifier computation caused by a large number of support vectors by using a predefined model. S-SVM avoids the slow computation problem caused by a large number of support vectors by using a predefined model.

The predefined model selects a representative set of basic elements $C = \{c_1, c_2, \ldots, c_m\}$ from the sample data to reduce the size of the sample data set, and estimates the normal vector ω, and then calculates the discriminant function to construct the classifier. The expression of the normal vector estimated according to Equation (16) is as follows.

$$\omega \simeq \sum_{i=1}^{m} \beta_i \varphi(c_i) \tag{16}$$

Where $\varphi(\cdot)$ is the mapping function, β is similar to the Lagrange multiplier, and the objective function is similar to Eq. (17), denoted as.

$$\begin{gathered} \min_{\beta} \frac{1}{2} \beta^T K_C \beta + C \sum_{i=1}^{m} \xi_i \\ \text{s.t. } y_i\left(\beta^T K_{ij} + b\right) \geq 1 - \xi_i \forall i = 1, 2, \ldots, m \\ \xi_i \geq 0, i = 1, 2, \ldots, m \end{gathered} \tag{17}$$

Where the matrix K_C denotes the $n \times n$ kernel matrix of the basic elements, i.e., $\left(K_C\right)_{i,j} = k\left(c_i, c_j\right), \forall i, j = 1, 2, \ldots, n, K_{ij} = k\left(x_i, c_j\right)$. The discriminant function is constructed as described in the previous section.

$$f(x_i) = \sum_{j=1}^{m} \beta_j k\left(x_i, c_j\right) + b \tag{18}$$

It can be seen that by limiting the size of the basic element set m, the complexity and operation speed of the classifier can be effectively limited. However, the element set C plays an important role for this kind of classifier, which has a great influence on

https://doi.org/10.17993/3ctecno.2024.v13n1e45.99-128

the classification performance and accuracy, and a processing tool that can accurately select the element set C is needed.

2.2.2. SEMI-PARAMETRIC SUPPORT VECTOR MACHINES BASED ON LEAST SQUARES

For the selection of the basic element set, this subsection adopts the sparse greedy matrix approximation, SGMA algorithm, and introduces the iterative reweighted least squares algorithm, IRWLS, to calculate the weights of the kernel function.

The kernel function used in this paper is Gaussian kernel function, as shown in Eq. (19).

$$k\left(x_i, x_j\right) = \exp\left(-\frac{\| x_i - x_j \|^2}{2\sigma^2}\right) \tag{19}$$

The kernel matrix K of the sample data set $T = \left\{x_1, x_2, \ldots, x_n\right\}$ is denoted.

$$K = \begin{bmatrix} k\left(x_1, x_1\right) & \cdots & k\left(x_1, x_j\right) & \cdots & k\left(x_1, x_n\right) \\ \vdots & \ddots & \vdots & \ddots & \vdots \\ k\left(x_i, x_1\right) & \cdots & k\left(x_i, x_j\right) & \cdots & k\left(x_i, x_n\right) \\ \vdots & \ddots & \vdots & \ddots & \vdots \\ k\left(x_n, x_1\right) & \cdots & k\left(x_n, x_j\right) & \cdots & k\left(x_n, x_n\right) \end{bmatrix} \tag{20}$$

In this paper, we use the hinge loss function to construct a soft interval classifier.

$$\ell_{\text{hinge}}(y) = \max(0, 1 - y) \tag{21}$$

Where y is the predicted classification output.

2.2.3. SPARSE GREEDY MATRIX APPROXIMATION

Given that the semiparametric support vector machine needs to select a suitable basic element set C, this section introduces the sparse greedy matrix approximation algorithm to find the element set C. The basic element set Cselected by using the SGMA algorithm can represent the whole sample dataset with the most representative features, which is very useful for solving the support vectors, constructing classifiers, and improving the classification performance.

https://doi.org/10.17993/3ctecno.2024.v13n1e45.99-128

For the sample dataset $T = \{x_1, x_2, \ldots, x_n\}$, a subset $N = \{x_1, x_2, \ldots, x_k\}$ is randomly selected; for optimal performance, the range of k needs to be larger than . $log0.05/log0.95 = 59$ The optimal set of basic elements $C = \{c_1, c_2, \ldots, c_m\}$ is selected by the elements in the subset N.

Assuming that the kernel function of the column vectors in the subset N is estimated to be $k(x_i, .)$, set a value $\lambda, k(x_i, .)$ to be a linear combination of λ and the kernel function $k(c_i, .)$, of the elements in C.

$$k(x_i, .) = \sum_{j=1}^{\kappa} \lambda_{ij} k(c_i, .) \tag{22}$$

Where λ_{ij} is noted as the weight value.

The approximation error of the weights λ_{ij} can be determined by the kernel function of the kernel matrix trace of the sample dataset T and the column vectors in the subset N as $k(x_i, .)$.

$$\mathrm{Err}(\lambda) = \mathrm{tr}K - \sum_{i=1}^{n} \sum_{j=1}^{m} \lambda_{ij} k(x_i, c_j) \tag{23}$$

After the new element c_{m+1} is added to the basic element set C by the SGMA algorithm, the new weight error is shown in Eqs. (24) and (25).

$$\begin{aligned} &\mathrm{Err}(\lambda^{n,m+1}) = \mathrm{Err}(\lambda^{n,m}) - \eta^{-1} \parallel K^{n,m} z - k_{Sn} \parallel^2 \\ &(k_{NC})_i = k(x_i, c_{m+1}) \\ &z = K_c^{-1} \cdot k_{mc} \\ &\eta = 1 - z^T k_{mc} \\ &(k_{mC})_i = k(c_i, c_{m+1}) \end{aligned} \tag{24}$$

$$ED = \mathrm{Err}(\lambda^{n,m}) - \mathrm{Err}(\lambda^{n,m+1}) \tag{25}$$

K_C is the $m \times m$ kernel matrix of the basic element K, and $K^{n,m}$ is the $n \times m$ kernel matrix of the subset N and the basic element set C.

From the above analysis, the SGMA algorithm can calculate the element with the maximum ED value in the data set by the formula (25), and add this metamethod to the basic data set C, so as to find out a group of subsets that can more accurately represent the distribution of the whole feature space.

https://doi.org/10.17993/3ctecno.2024.v13n1e45.99-128

2.2.4. ITERATIVE REWEIGHTED LEAST SQUARES

The iterative reweighted least squares, IRWLS, process is a solution method that has been widely used in the field of support vector machines. Compared with the weighted least squares algorithm, IRWLS can gradually correct for the effects of anomalous sample data and set the weights always within a relatively optimal range.

For the Lagrangian function with the penalty factor C_p added.

$$L(\omega, b, a, \xi, \mu) = \frac{1}{2} \parallel \omega \parallel^2 + C_p \sum_{i=1}^{n} \xi_i + \sum_{i=1}^{n} a_i \left(1 - \xi_i - y_i\left(\omega^T \varphi(x_i) + b\right)\right) - \sum_{i=1}^{n} \mu_i \xi_i \tag{26}$$

By taking the partial derivation of Eq. (26) and eliminating the term about ξ_i and calculating $C_p = a_i + \mu_i$, Eq. (27) is converted as shown below.

$$\begin{aligned} L(\omega, b, a, \xi, \mu) &= \frac{1}{2} \parallel \omega \parallel^2 + \sum_{i=1}^{n} a_i \left(1 - y_i\left(\omega^T \varphi(x_i) + b\right)\right) \\ &= \frac{1}{2} \parallel \omega \parallel^2 + \frac{1}{2} \sum_{i=1}^{n} \frac{2a_i}{1 - y_i\left(\omega^T \varphi(x_i) + b\right)} \left(y_i\left(\omega^T \varphi(x_i) + b\right)\right)^2 \\ &= \frac{1}{2} \parallel \omega \parallel^2 + \frac{1}{2} \sum_{i=1}^{n} a_i e_i^2 \end{aligned} \tag{28}$$

In which:

$$e_i = y_i\left(\omega^T \varphi(x_i) + b\right) \tag{29}$$

$$\alpha_i = \frac{2a_i}{1 - y_i\left(\omega^T \varphi(x_i) + b\right)} \tag{30}$$

e_i is denoted as the error of the sample data points, and α_i is denoted as the weight coefficient associated with it. Substituting $\omega \simeq \sum_{i=1}^{n} \beta_i \varphi(x_i)$ into Eq. (30) to obtain Eq. [112] with respect to α_i, the objective function is obtained.

$$\text{s.t.e } e_i = y_i - \left(\sum_{j=0}^{m} \beta_i K(x_i, c_i) + b\right) \tag{31}$$

$$\alpha_i = \begin{cases} 0, & y_i e_i \leq 0 \\ \dfrac{C_p}{e_i y_i}, & y_i e_i > 0 \end{cases} \tag{32}$$

https://doi.org/10.17993/3ctecno.2024.v13n1e45.99-128

Determine the weight β through equation (33).

$$\begin{bmatrix} K_C + K_{sC}^T D_a K_{sc} & K_{sc}^T D_\alpha 1 \\ 1^T D_a K_C^{-1} & 1^T D_a 1 \end{bmatrix} \begin{bmatrix} \beta \\ b \end{bmatrix} = \begin{bmatrix} K_{sc}^T D_\alpha y \\ 1 D_a y \end{bmatrix} \tag{33}$$

Where $\left(K_C\right)_{ij} = k\left(c_i, c_j\right), K_{SC} = k\left(x_i, c_j\right), \left(D_\alpha\right)_i = \alpha_i$, vectors $1 = [1, \ldots, 1]^T$, $y = \left[y_1, y_2, \ldots, y_n\right]^T$

The iterative process allows each round of training and learning to gradually correct the weight values, so that the weights α_i and β eventually converge to a fixed value, and the iterative calculation steps are as follows.

Step 1: Pre-set a weight α_i, solve the least squares problem to obtain β.

Step 2: Based on the correlation between weight BB and α_i, re-calculate the value of α_i by calculating weight β.

Step 3: Repeat the first two steps until the weights β and α_i converge to a fixed convergence value.

At this point, the discriminant function of the classifier is:

$$f\left(x_i\right) = \sum_{j=1}^{m} \beta_j k\left(x_i, c_j\right) + b \tag{34}$$

2.2.5. WAVELET TRANSFORM

The continuous wavelet transform of the function $f(t)$ is shown in equation (35).

$$W(f, a, b) = \frac{1}{\sqrt{a}} \int_{-\infty}^{+\infty} f(t) \psi^* \left(\frac{t-b}{a} \right) dt \tag{35}$$

Where, a is the scale factor, b is the translation factor and $\psi(t)$ is the mother wavelet.

Continuous wavelet transform can accurately extract the characteristics of the signal, but in each possible scale discrete points to calculate the wavelet coefficients, will be a huge project. if only a small part of these scales, and part of the time point, will greatly reduce the workload, and without loss of accuracy, the use of such an approximation will be obtained by the discrete wavelet transform, the definition of which is shown in equation (36).

https://doi.org/10.17993/3ctecno.2024.v13n1e45.99-128

$$\mathrm{DWT}(f,m,n)=\frac{1}{\sqrt{a_0^m}}\sum_k f(k)y^*\left(\frac{n-ka_0^m}{a_0^m}\right) \tag{36}$$

In Eq. (36), the parameters a and b of continuous wavelet transform are replaced by a_0^m and ka_0^m, k and MM are integers, and A02 is taken in general. The wavelet decomposition tree of the discrete wavelet transform is shown in Fig. 2. The original signal sequence of SN is shown in Fig. 2. CA_k denotes the low-frequency coefficients of the decomposition of the k layer, and CD_k denotes the high-frequency coefficients of the k decomposition. The signal components obtained from the decomposition of the decomposition coefficients of each layer by the single-branch reconstruction are denoted as a_k and D_k, and then the original signal $S(n)$ is the sum of the signal components obtained by the reconstruction, and the formula is as follows.

$$x(n)=D_1+A_1=D_1+D_2+A_2=\sum_{j=1}^{n}D_j+A_n \tag{37}$$

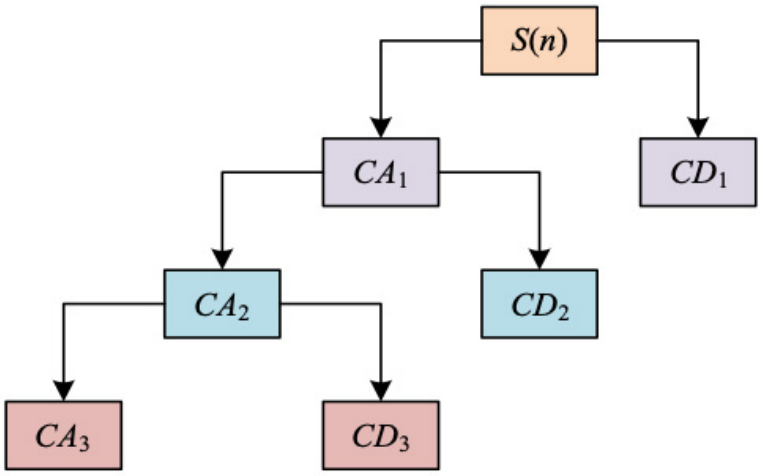

Figure 2 The wavelet decomposition tree

2.2.6. SHANNON INFORMATION ENTROPY AND WAVELET SINGULAR ENTROPY

Shannon information entropy and its state characteristics can be expressed by a variable X that takes a finite number of values, the probability that the state characteristics of the source take the value of x_j is $p_j=P\left\{X=x_j\right\}j=1,\cdots,L$ and $\sum_{j=1}^{L}p_j=1$, then $I_j=\log\left(1/p_j\right)$ represents the information obtained from the j result of X, and the information entropy is defined as shown in Equation (38).

https://doi.org/10.17993/3ctecno.2024.v13n1e45.99-128

$$H(X) = -\sum_{j=1}^{L} p_j \log\left(p_j\right) \tag{38}$$

Wavelet singular entropy is a new data processing method obtained by combining wavelet transform with Shannon's information entropy theory, which is defined as follows.

$$W_k = \sum_{i=1}^{k} \Delta p_i \tag{39}$$

In Eq. (40), Δp_i is the incremental wavelet singular entropy of order j.

$$\Delta p_i = -\left(\lambda_i / \sum_{j=1}^{l} \lambda_j\right) \log\left(\lambda_i / \sum_{j=1}^{l} \lambda_j\right) \tag{40}$$

The $\lambda_i (i = 1, \cdots, l)$ is calculated as follows.

After the signal $S(n)$ wavelet decomposition and reconstruction of the components at the $j(j = 1, \cdots m)$th scale is $D_j(n)$, then the m components of the signal $S(n)$ can form a $m \times n$ matrix $D_{m\times n}$, by the theory of signal singular value decomposition, for the above matrix $D_{m\times n}$, there exists a $m \times l$-dimensional matrix U and a $l \times l$ -dimensional diagonal matrix Λ and a $l \times n$-dimensional matrix V, so that the matrix Dmxn decomposition is as shown in Eq. (41).

$$D_{m\times n} = U_{m\times 1} \Lambda_{I\times 1} V_{l\times n} \tag{41}$$

Where, $\lambda_i (i = 1, \cdots, l)$ is the element on the main diagonal of the diagonal matrix Λ, i.e., the singular value of the matrix $D_{m\times n}$ formed after the signal $S(n)$ is decomposed by the wavelet decomposition of the m layer and reconstructed.

2.2.7. CABLE FAULT DETECTION STRATEGY BASED ON WAVELET SINGULAR ENTROPY AND S-SVM MODELS

In this section, wavelet singular entropy and semiparametric support vector machine are combined and applied to cable fault detection, and the cable fault detection strategy based on wavelet singular entropy and S-SVM model is shown in Fig. 2. firstly, the cable current signal is extracted, then wavelet singular entropy is used to decompose the signal, extract the meaningful sub-signal components, and then the correlation analysis is used to filter the components to reconstruct the fault signal, and then wavelet singular entropy is used to reduce the influence of non-Gaussian noise on the fault signal, extract the wavelet energy entropy of harmonic components as feature vectors, and then the fault sample data is inputted into the S-SVM model to be trained. Then the wavelet singular entropy is used to reduce the

https://doi.org/10.17993/3ctecno.2024.v13n1e45.99-128

effect of non-Gaussian noise on the fault signal, and the wavelet energy entropy of the harmonic components is extracted and used as the feature vectors. After that, the fault sample data are inputted into the S-SVM model for training, and the S-SVM model is finally used to recognize and diagnose the test samples.

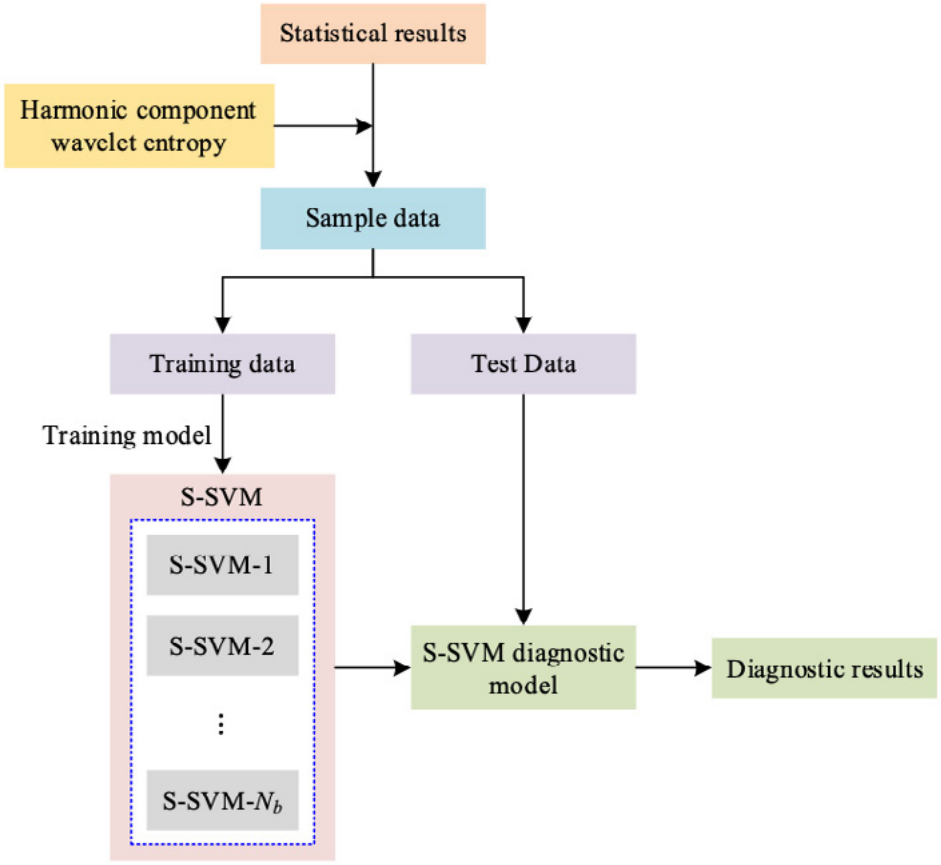

Figure 3 Cable fault detection strategy based on wavelet singular entropy and S-SVM model

3. ANALYSIS OF INTELLIGENT CABLE FAULT DETECTION RESULTS CONSIDERING CURRENT HARMONIC FEATURES

3.1. ANALYSIS OF INTELLIGENT DETECTION RESULTS OF CABLE LINE DETERIORATION FAULTS

3.1.1. HARMONIC FEATURE EXTRACTION FOR CABLE LINE DEGRADATION

In this section, according to the structural characteristics of the cable, 40,000 sets of harmonic diagnostic data of the same power cable are selected, and the harmonic content of the main part of the cable from the 2nd to the 10th harmonic is multiplied with its corresponding contribution rate, and 9 harmonic vectors are obtained as the

https://doi.org/10.17993/3ctecno.2024.v13n1e45.99-128

input data, and the degree of deterioration of the insulation, shielding, protective layer and cable joints are derived through the improved HHT transformation model. The energy spectrum of the harmonic vectors of different parts of the cable is shown in Fig. 4, and the relative energy of each harmonic is 1. The relative energies of the harmonic vectors are obviously different in diagnosing the operation status of different parts of the cable, the operation status of the cable insulator mainly depends on the change of the 2nd harmonic vector, with the relative energy value of 0.32, and the operation status of the shielding layer mainly depends on the change of the 2nd, 3rd, and 5th harmonic vectors, with the relative energy value of 0.24, 0.25, 0.2, 0.5, and 0.6, respectively. 0.25 and 0.2 respectively, and the operating state of the protective layer and the roving state of the cable joints mainly depends on the changes of the 2nd, 4th, 7th, 8th and 9th harmonic vectors, with the relative energy values of 0.3, 0.25 and 0.26, 0.26, 0.3 respectively. The harmonic vectors obtained based on the improved HHT transformation model completely characterize the operating state of the different parts of the cables.

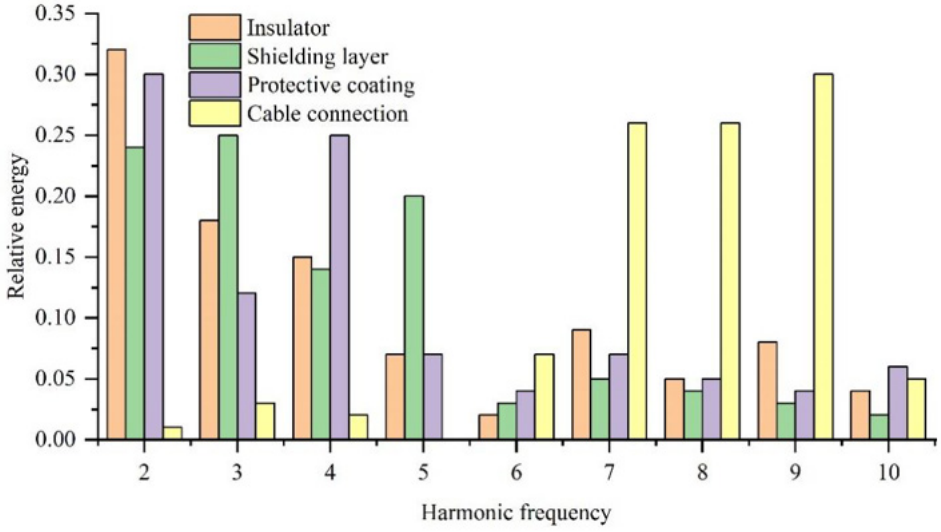

Figure 4 The shoe wave vector energy spectrum of the different parts of the cable

3.1.2. ANALYSIS OF CABLE LINE DETERIORATION IDENTIFICATION TEST RESULTS

In this section, based on the wavelet singular entropy and S-SVM model to identify and detect the degradation of cable lines, in order to verify the accuracy of the wavelet singular entropy and S-SVM model, the harmonic characteristics database of different fault loss currents of cables is formed by taking the harmonic total aberration rate, the fundamental content and the harmonic contents of each harmonic as the characteristics.Firstly, we extracted the sample data of the loss currents in the database to form the sample data set of the wavelet singular entropy and S-SVM model. Then some data in the sample data set are randomly extracted as the training sample set, and the rest of the data in the sample data set are used as the test sample set. finally, different ratios of the training set to the test set are set, and

https://doi.org/10.17993/3ctecno.2024.v13n1e45.99-128

different numbers of test samples are taken to identify the deterioration of cables with the wavelet singular entropy and the S-SVM model trained in the above steps. red part indicates the classification of the predicted test set, and blue part indicates the classification of the actual test set. red part indicates the classification of the predicted test set, and blue part indicates the classification of the actual test set. red part indicates the classification of the actual test set. The red part indicates the classification of the predicted test set, and the blue part indicates the classification of the actual test set, and the coincidence of the red part and the blue part indicates that the test set data matches with the prediction result, and the prediction result is accurate, and vice versa.The accuracy results of the wavelet singular entropy and S-SVM models with different ratios of the training set to the test set are shown in Fig. 5, and the results of the accuracy results of the models with the ratio of the training set to the test set 6:4, 7:3, 8:2, and 9:1 are shown in Figs. 5(a) to (d) respectively. Vertical coordinates 1, 2, 3 and 4 indicate the degradation of insulator, shield, protective layer and cable connector, respectively.When the ratio of training set to test set is 6:4, there are 12 groups of prediction failures, 6 groups of samples predicted the protective layer to be insulator, and 4 groups of samples predicted the shield to be insulator, with an identification accuracy of 93.93%.When the ratio of training set to test set is 7:3, there are 3 groups of samples predicted the protective layer sample to be insulator, with an identification accuracy of 93.93%. When the ratio of training set to test set is 7:3, there are 3 groups of protective layer samples predicted to be shielding layer and 2 groups of shielding layer samples predicted to be insulators, the recognition accuracy is 94.38%. when the ratio of training set to test set is 8:2, there are 1 group of protective layer and 1 group of shielding layer samples predicted to be insulators, the recognition accuracy is 96.58%. when the ratio of training set to test set is 9:1, there is only 1 group of protective layer sample predicted to be insulators, the recognition accuracy is 97.36%. The more training samples, the higher the accuracy of wavelet singular entropy and S-SVM model in recognizing different cable line degradation, and the recognition rate is above 93%, which indicates that this model can well identify the categories of cable line degradation.

https://doi.org/10.17993/3ctecno.2024.v13n1e45.99-128

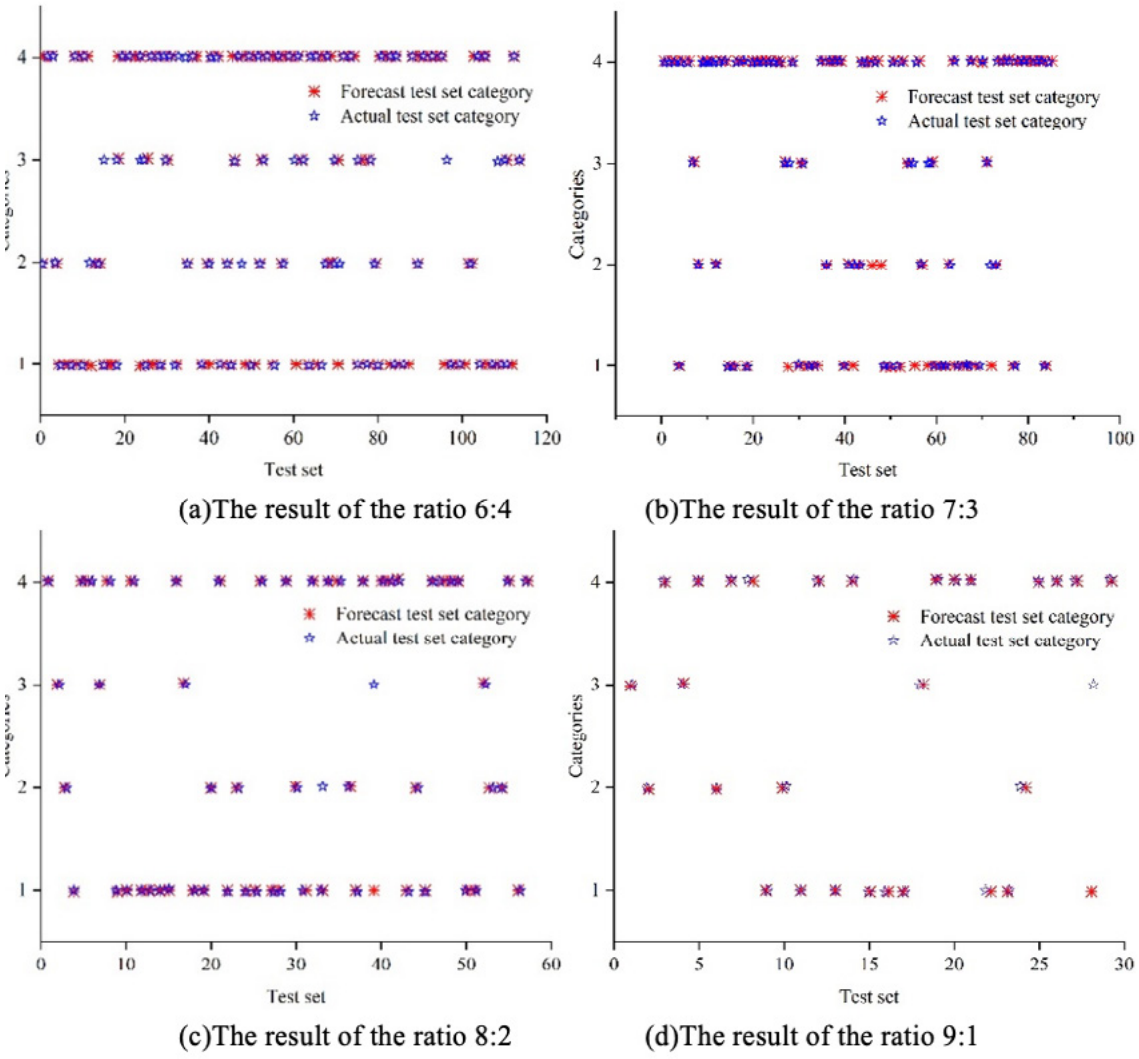

Figure 5 Results of different training sets and test sets

3.2. ANALYSIS OF INTELLIGENT DETECTION RESULTS OF CABLE SHORT-CIRCUIT FAULTS

In order to provide data support for cable fault diagnosis, this paper adopts the 10KV cable line model to construct the fault data set, and utilizes the electrical components in the tool library to build the simulation circuit.

3.2.1. CABLE SHORT CIRCUIT FAULT ANALYSIS

Cable short-circuit fault is the largest proportion of cable faults occurring, cable a phase connected to another phase or one of the phases connected to the earth is called a short-circuit fault, in the case of mixed faults do not take into account the occurrence of 10 types of faults may occur: A_G, B_G, C_G were A-phase, B-phase and C-phase ground faults, AB, AC, BC, respectively, on behalf of AB, AC two-phase and BC two-phase short-circuit faults, AB_G, AC_G, BC_G were AB-phase, AC phase and BC two-phase short-circuit ground faults, ABC is a three-phase short-circuit fault,

https://doi.org/10.17993/3ctecno.2024.v13n1e45.99-128

ABC is a three-phase short circuit. AB_G, AC_G, BC_G are AB phase, AC phase and BC two-phase short-circuit ground faults, and ABC is three-phase short-circuit faults.Figure 6 shows the current waveform curves of the cable in normal operation and various short-circuit faults, and Fig. 6(a)~(d) shows the current waveform curves of the cable in normal operation, the single-phase grounded short-circuit faults, and two-phase indirect short-circuit current waveforms, and Fig. 6(a)~(d) shows the current waveform curve of the cable in normal operation, single-phase ground faults, and two-phase short-circuit faults, and Fig. 6(a)~(d) shows the current waveform curves of the cable in normal operation. Indirect ground short-circuit current waveform curve, three-phase ground short-circuit waveform curve. cable normal operation current waveform is more symmetrical, the overall current between -10K-10K amperes. cable short-circuit faults, short-circuit current is lower than the normal current. single-phase ground short-circuit, fault A-phase current in the 0.07s current is smaller than the non-fault B, C-phase current, and the waveform is more chaotic. two-phase short circuit in the 0.075s, the AB phase current is lower than the non-fault C phase current, AB two short-circuit faults occur. three-phase short-circuit fault, in 0.075s, the three-phase current is lower than the normal current, and the three-phase current sum is equal to zero.

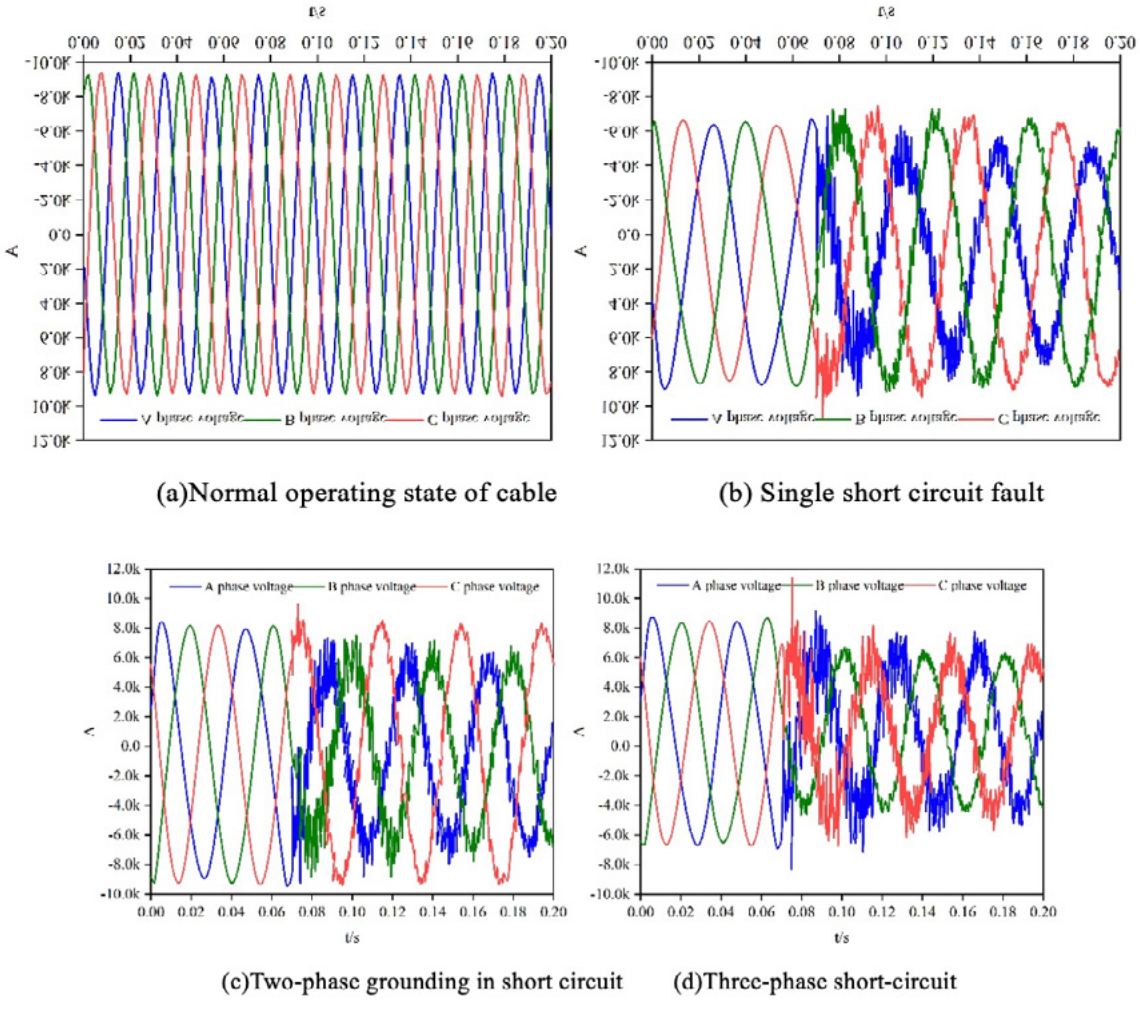

Figure 6 The current waveform of the cable's various circuited faults

https://doi.org/10.17993/3ctecno.2024.v13n1e45.99-128

3.2.2. HARMONIC FEATURE EXTRACTION FOR CABLE SHORT-CIRCUIT FAULTS

In this section of the experiment, the sampling frequency is set to 12.8kHz, the sampling time is 0.2s, and the fault is imposed after 0.05s of the system's normal operation state, each simulation samples 2780 points of voltage, each line has three phases, and each line collects 8670 points, i.e., the length of each sample is 8670, and then collects the operation state of 10 cables, 80% of them are used as training samples, 20% as test samples, and 18 harmonic vectors are obtained by using the improved HHT transform model. Figure 7 shows the energy spectrum of harmonic vector during various short-circuit faults of cable. 20% are used as test samples, and 18 harmonic vectors are obtained by using the improved HHT transform model. Fig. 7 shows the energy spectrum of harmonic vectors in various short-circuit faults of cables. In single-phase cable short-circuit, phase A mainly looks at the 1st and 9th harmonics, with the relative energy values of 0.18 and 0.12, respectively, and phases B and C mainly look at the 1st and 2nd harmonics, with the relative energy values of 0.19 and 0.12, 0.24 and 0.14, respectively. Two-phase cable short-circuit mainly looks at the 1st and 2nd harmonics, with the relative energy values of 0.19 and 0.12, 0.24 and 0.14, respectively. When two-phase cable is short-circuited, phase A mainly looks at the 18th harmonic with a relative energy value of 0.38, phase B mainly looks at the 13th and 16th harmonics with relative energy values of 0.17 and 0.14, and phase C mainly looks at the 15th harmonic with a relative energy value of 0.21. When three-phase cable is short-circuited, phase A mainly looks at the 2nd harmonic with a relative energy value of 0.05, phase B mainly looks at the 1st and 2nd harmonics with relative energy values of 0.19 and 0.12, and phase B mainly looks at the 1st and 2nd harmonics with relative energy values of 0.19 and 0.14, and phase C mainly looks at the 1st and 2nd harmonics with relative energy values of 0.19 and 0.14 respectively. The relative energy values are 0.19 and 0.13 for phase B, and 0.13 and 0.1 for phase C, mainly for the 2nd and 3rd harmonics.

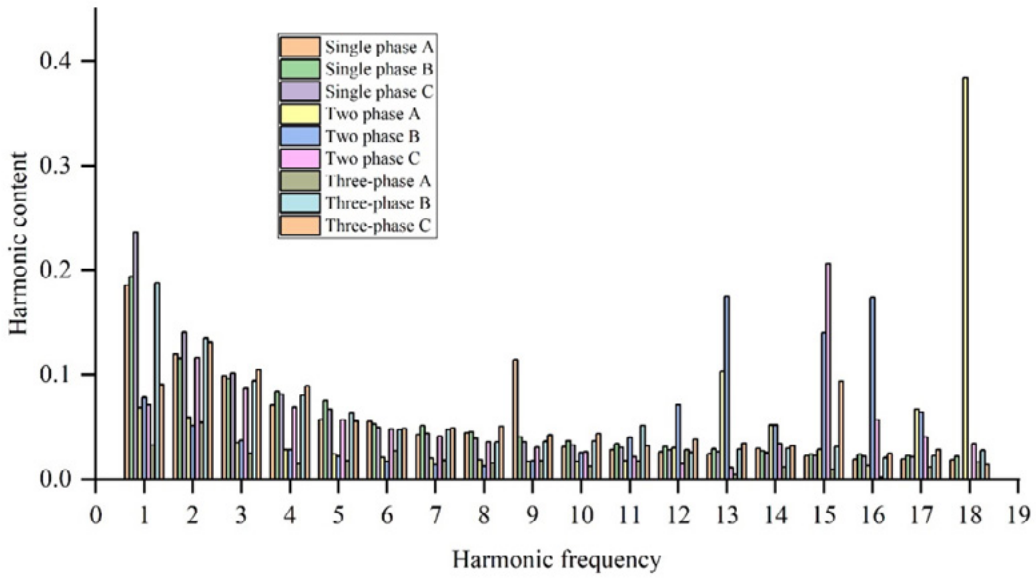

Figure 7 The harmonic energy spectrum of all kinds of short-circuit failures of the cable

https://doi.org/10.17993/3ctecno.2024.v13n1e45.99-128

3.2.3. IDENTIFICATION AND DETECTION RESULTS OF CABLE SHORT-CIRCUIT FAULTS

This section extracts local features of the input target based on wavelet singular entropy and S-SVM model, achieving target detection and improving diagnostic efficiency. Figure 7 shows the confusion matrix of the cable fault diagnosis model, where the vertical axis represents the true category of the cable fault signal and the horizontal axis represents the predicted category of the network for the cable fault signal, The diagonal values on the matrix represent the probability of correctly classifying cable fault signals. Wavelet singular entropy and S-SVM models can fully identify 10 types of cable short circuit faults. For A_ G, B_ G, C_ G, AB, AC, BC, AB_ G, AC_ G, BC_ The correct classification probabilities for 10 types of short-circuit faults, including G and ABC, are 0.94, 0.95, 0.96, 0.96, 0.98, 0.99, 0.94, 0.92, and 1, respectively. Although the correct classification probability for BC phase short-circuit grounding is relatively low, the overall probability is above 90%, indicating that the diagnosis of cable faults based on wavelet singular entropy and S-SVM model is completely feasible

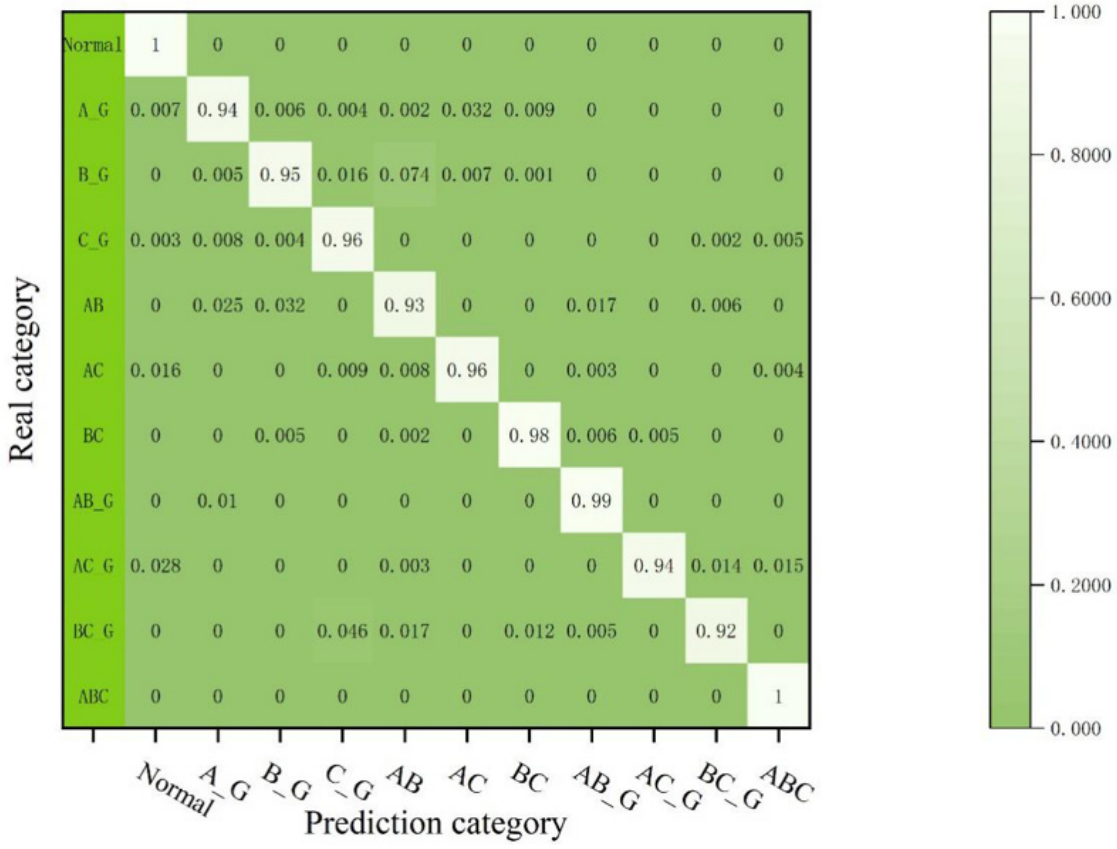

Figure 8 Confusion matrix of cable fault diagnosis model

https://doi.org/10.17993/3ctecno.2024.v13n1e45.99-128

3.3. ANALYSIS OF INTELLIGENT DETECTION RESULTS OF CABLE FAULTS

In order to verify the diagnostic effect of wavelet singular entropy and S-SVM model on all faults of cables, 180 samples are selected for test experiments in this section. The maximum error of wavelet singular entropy and S-SVM model on the test samples is 0.5329, only two samples have the absolute error value more than 0.5, and the other samples have the absolute error value lower than 0.5, and the average error is 0.1124.Among 180 sets of test samples, the correct rate of wavelet singular entropy and S-SVM model to diagnose various cable faults reached 98.04%, and the performance is good. In 180 sets of test samples, the correct rate of the wavelet singular entropy and S-SVM model in diagnosing various cable faults reaches 98.04%, which is good, and the wavelet singular entropy and S-SVM model can be used in the actual cable fault diagnosis.

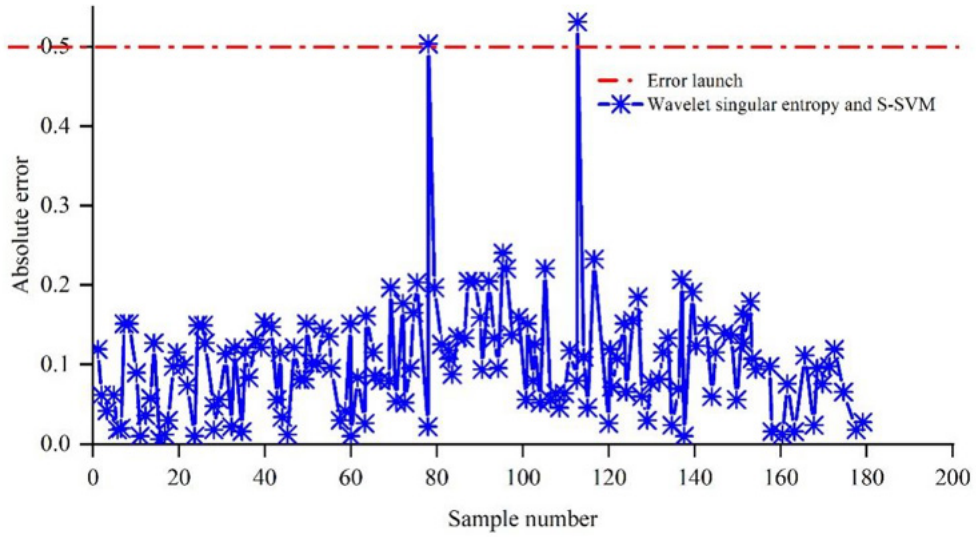

Figure 9 Wavelet singular entropy and S-SVM model diagnose cable fault curve

4. CONCLUSION

In this paper, by improving the envelope fitting algorithm of HHT algorithm, the HHT transform model is proposed to extract the current harmonic features of the cable. wavelet singularity algorithm and S-SVM algorithm are utilized to construct into the wavelet singular entropy and S-SVM model for detecting the faults of the cables. the experimental results are as follows.

In the detection of cable line deterioration, the current harmonic vectors characterize the operation status of different parts of the cable, and the operation status of cable insulator, shield, protective layer and cable joints are shown in the changes of 2nd, 2nd, 3rd, 5th, 2nd, 4th and 7th, 8th, 9th harmonic vectors, respectively, and the accuracy of the Wavelet Singularity Algorithm and S-SVM algorithm on the detection of the cable line deterioration is 93.93%, 94% and 94%, respectively. are 93.93%, 94.38%, 96.58% and 97.36%.

https://doi.org/10.17993/3ctecno.2024.v13n1e45.99-128

In the detection of cable short circuit faults, the current of different short circuit faults in the cable is lower than the normal current, and in the case of three-phase short circuit faults, the three-phase currents add up to 0. For the extraction of the different short circuit current harmonics, in the case of a single-phase short circuit in the cable, the operating state of phases A, B, and C is shown in the first and ninth, first and second, and first and second harmonics of the current respectively, in the case of a two-phase short circuit in the cable, the operating state of phases A, B, and C is shown in the 18th, 13th, and 16th, and 15th harmonics of the current respectively. When three-phase cable is short-circuited, the operating states of phases A, B and C are characterized by 2, 1 and 2, 2 and 3 harmonic vectors, respectively. The wavelet singularity algorithm and S-SVM algorithm have an accuracy of more than 92% in identifying 10 different cable short-circuit faults, such as A_G, B_G, C_G, AB, AC, BC, AB_G, AC_G, BC_G, ABC, and so on.

Overall for cable fault detection, the wavelet singularity algorithm and S-SVM algorithm have reached 98.04% correct rate for detecting all kinds of pegged accounts of cables, and the error value is only more than 0.5 for two groups of data out of 180 groups of sample data. The improved HHT transform model and the wavelet singular entropy and S-SVM models proposed in this paper have high accuracy and practicability, and provide a a new method.

REFERENCES

(1) Otsu, H., Yone, Y., Takahashi, E., & Koike, K. (2017). Supply and demand situation of wood-chips before and after the increase in power-plant demand in the Chugoku region. Journal of Forest Economics, 63.

(2) Ros, A., & J. (2017). An econometric assessment of electricity demand in the United States using utility-specific panel data and the impact of retail competition on prices. Energy Journal.

(3) Nguyen, T. T., Lee, W. G., Kim, H. M., Yang, H. S., & Sciubba, E. (2020). Fault analysis and design of a protection system for a mesh power system with a co-axial HTS power cable. Energies, 13(1), 220.

(4) Zhang, Z.-h., Xu, B.-y., Crossley, P., & et al. (2018). Positive-sequence-fault-component-based blocking pilot protection for closed-loop distribution network with underground cable. International Journal of Electrical Power & Energy Systems.

(5) Zhang, Z., Chen, Q., Xie, R., & Ranran. (2019). The fault analysis of PV cable fault in DC microgrids. IEEE Transactions on Energy Conversion, 34(1), 486-496.

(6) Cozza, A. (2019). Never trust a cable bearing echoes: understanding ambiguities in time-domain reflectometry applied to soft faults in cables. IEEE Transactions on Electromagnetic Compatibility.

(7) Khavari, S., Dashti, R., Shaker, H. R., & Santos, A. (2020). High impedance fault detection and location in combined overhead line and underground cable distribution networks equipped with data loggers. Energies, 13.

(8) Popovi, L. M. (2018). Reduction of the fault current passing through the grounding system of an HV substation supplied by cable line. International Journal of Electrical Power & Energy Systems, 99, 493-499.

https://doi.org/10.17993/3ctecno.2024.v13n1e45.99-128

(9) Nguyen, T. T., Lee, W. G., Kim, H. M., Yang, H. S., & Sciubba, E. (2020). Fault analysis and design of a protection system for a mesh power system with a co-axial HTS power cable. Energies, 13(1), 220.

(10) Peake, L. (2018, May). Making cable fault location even easier. Electrical Engineering.

(11) Baranowski, J., Grobler-Dbska, K., & Kucharska, E. (2021). Recognizing VSC DC cable fault types using Bayesian functional data depth. Energies, 14.

(12) Liu, X., & Wang, H. (2020). Analytical expression for estimation of the fault location in cable line. IET Science, Measurement & Technology, 14(8).

(13) Xuebin, Q., Yizhe, Z., Wang, M., Gang, D., Jun, G., & Pai, W. (2018). A cable fault recognition method based on a deep belief network. Computers & Electrical Engineering, 71, 452-464.

(14) Cataldo, A. C. G. (2021). A new measurement algorithm for TDR-based localization of large dielectric permittivity variations in long-distance cable systems. Measurement, 174(1).

(15) Wang, F., Yuan, G., Guo, C., & Li, Z. (2022). Research on fault diagnosis method of aviation cable based on improved Adaboost. Advances in Mechanical Engineering, 14.

(16) Sian, H. W., Kuo, C. C., Lu, S. D., & Wang, M. H. (2023). A novel fault diagnosis method of power cable based on convolutional probabilistic neural network with discrete wavelet transform and symmetrized dot pattern. IET Science, Measurement & Technology.

(17) Marriott, N. (2021, June). Megger launches cable fault locator. Electrical Engineering.

(18) Lowczowski, K., Lorenc, J., Zawodniak, J., & Dombek, G. (2020). Detection and location of earth fault in MV feeders using screen earthing current measurements. Energies, 13.

(19) Hu, C., Huang, Y., & You, Z. (2019). Ship cable fault info acquisition model based on auto recognition. Journal of Coastal Research, 94, 510-514.

(20) Lai, Q., Chen, J., Hu, L., Cao, J., & Zhu, N. (2020). Investigation of tail pipe breakdown incident for 110 kV cable termination and proposal of fault prevention. Engineering Failure Analysis, 108, 104353.

(21) Liu, N., Fan, B., Xiao, X., & Yang, X. (2019). Cable incipient fault identification with a sparse autoencoder and a deep belief network. Energies, 12(18), 3424.

(22) Wang, Y., Lu, H., Xiao, X., Yang, X., & Zhang, W. (2019). Cable incipient fault identification using restricted Boltzmann machine and stacked autoencoder. IET Generation Transmission & Distribution, 14(7).

(23) Qu, K., Zhang, W., Zhang, S., Xiao, X., Xi, Y., & Zhang, H. (2022). Model-free underground cable incipient fault location using two-terminal zero-sequence measurements. International Journal of Electrical Power & Energy Systems, 140, 108057.

(24) Kwon, G. Y., Lee, C. K., Lee, G. S., Lee, Y. H., Chang, S. J., & Jung, C. K. (2017). Offline fault localization technique on HVDC submarine cable via time–frequency domain reflectometry. IEEE Transactions on Power Delivery

https://doi.org/10.17993/3ctecno.2024.v13n1e45.99-128